

Scientific Paper

Doi: <http://dx.doi.org/10.1590/1809-4430-Eng.Agric.v42n4e20220030/2022>

QUANTITATIVE ANALYSIS AND HYPERSPECTRAL REMOTE SENSING INVERSION OF RICE CANOPY SPAD IN A COLD REGION

Yinjiang Jia¹, Huaijing Zhang¹, Xiaoyu Zhang¹, Zhongbin Su^{1*}

^{1*} Corresponding author. Northeast Agricultural University/Harbin, China.

E-mail: suzb001@163.com | ORCID ID: <https://orcid.org/0000-0002-8966-8933>

KEYWORDS

SPAD, rice in cold region, hyperspectral image, spectral analysis, GA-BPNN.

ABSTRACT

This study used a spectral index method and an artificial intelligence algorithm to quantitatively analyze rice canopy soil and plant analyzer development (SPAD) based on ground nonimaging spectral data and UAV hyperspectral images to build a high-precision SPAD prediction model for nondestructive monitoring of the chlorophyll relative content of rice in cold regions. First, this study selected characteristic bands sensitive to SPAD using uninformative variable elimination and the successive projections algorithm. Then, the correlation between commonly used vegetation indices and SPAD was analyzed. Finally, this study constructed a back propagation neural network (BPNN) model, BPNN with particle swarm optimization (PSO-BPNN) model, and BPNN with genetic algorithm optimization (GA-BPNN) model, and then verified the reliability of these models. According to the results, GA-BPNN had the best predictive effect. The coefficient of the determination reached 0.818, and the root mean square error was 0.847. GA-BPNN model combined with UAV hyperspectral images were used for inversion mapping; the predicted range of SPAD was 33.1–41.2, which is in good agreement with the measured value (32.7–40.6). The inversion of regional rice canopy SPAD by nonimaging spectral data and UAV hyperspectral images had high credibility, which provided technical support for the scientific management of rice in a cold region.

INTRODUCTION

Chlorophyll content can effectively reflect the nutritional status of crops, monitoring the chlorophyll content of the rice canopy has important guiding significance for the evaluation of rice growth and yield prediction. Soil and plant analyzer development (SPAD) measures the relative level of crop chlorophyll content, particularly canopy chlorophyll content, which can reflect crop population traits and is frequently used to assess crop growth conditions, vegetation nutrient stress, and leaf nitrogen content (Song et al., 2021). Heilongjiang Province has excellent natural conditions and is China's largest rice-producing region. Accurately assessing rice SPAD is critical for guiding rice production and achieving higher quality and efficiency.

Near-earth spectroscopy technology is an effective method for detecting and obtaining crop nutrition status and

growth information (Guo et al., 2016) because of its high efficiency, low cost, lack of pollution, and ease of measurement (He et al., 2021). In recent years, domestic and foreign scholars have carried out a significant number of related research. Tang et al (2004) studied the hyperspectral and red-edge characteristics of rice canopy and leaves with different nitrogen supply levels, and then found that the biophysical parameters and pigment content of rice are comparable to R_{1200}/R_{550} , R_{990}/R_{550} , R_{800}/R_{550} , R_{750}/R_{550} , λ_{red} , S_{red} . With the rapid development of artificial intelligence, some researchers have begun to experiment with combining the spectral parameter method with an artificial intelligence algorithm to create crop nutrition models. Jiang et al (2015) used the PSR-3500 spectrometer to obtain spectrum data, selected three commonly used spectral indices for chlorophyll content inversion, and added the universal spectral index VI-UPD to establish a regression model, which achieved better accuracy and

¹ Northeast Agricultural University/Harbin, China.

Area Editor: Fabio Henrique Rojo Baio

Received in: 3-4-2022

Accepted in: 7-11-2022

stability. Li et al (2014) built a point model of rice canopy content inversion based on an improved random forest algorithm, with a coefficient of determination of 0.81. Due to the special soil background, climatic conditions, and growth cycle of cold regions, it is necessary to find adaptive models to evaluate the growth and nutrition of crops. Xu et al (2020) used the wavelet to establish the GA-ELM model, which provided a new idea for accurately detecting the nitrogen deficiency of japonica rice leaves. Tan et al (2017) calculated the eight vegetation indices based on spectral information and proposed a machine learning method of BPSO-SVR to predict nitrogen content, which can be used to detect nitrogen in rice at different growth stages in a cold region. Wen et al. (2019) considered the influence of the unsynchronized maize growth stage on the spectral model, verified the prediction ability of the published vegetation indices, the partial least squares regression, and the two-band optimal combinations algorithms.

Compared with the near-earth spectrometer, the image obtained by the airborne hyperspectral imager contains higher resolution, which can accurately reflect the spectral characteristics of the field crops themselves and the spectral differences between crops (Ma et al., 2020). Previous studies have shown that the spectrum and the combination of spectra show superiority. Even when only a limited amount of spectral reflectance data is available, high-precision prediction can be made through the spectral

index (Inoue et al., 2012). With the development of UAV platforms and hyperspectral imagers, image features, algorithms, and statistics are more widely used in the hyperspectral field. Zhu et al (2020) used the S185 airborne imaging spectrometer to obtain hyperspectral information on different growth cycles, different scales, and different crops and modeled them based on different algorithms. Yue et al (2019) selected texture features from the ultra-high-resolution images, combined with the vegetation index to estimate the biomass of winter wheat, and the correlation coefficient reached 0.89. Liu et al (2019) used a UHD185 airborne imaging spectrometer to study the hyperspectral characteristics of different growth stages and different nitrogen nutrient indices (NNI) to establish a hyperspectral model and carry out remote sensing prediction.

In the current study, most of the prediction of SPAD in rice comes from a single spectral data source, based on the “points” of the ground nonimaging spectral data or the “surfaces” of the low-latitude UAV spectral image data. However, few inversion studies combine the two scales. The primary research pathways followed in this study are shown in Fig 1. Based on spectral data of different scales, this study uses ground nonimaging spectral data for modeling, and UAV spectral image data for SPAD remote sensing inversion to verify the accuracy and robustness of the model, to provide technical support and reference for rice nutrition diagnosis, high-yield cultivation.

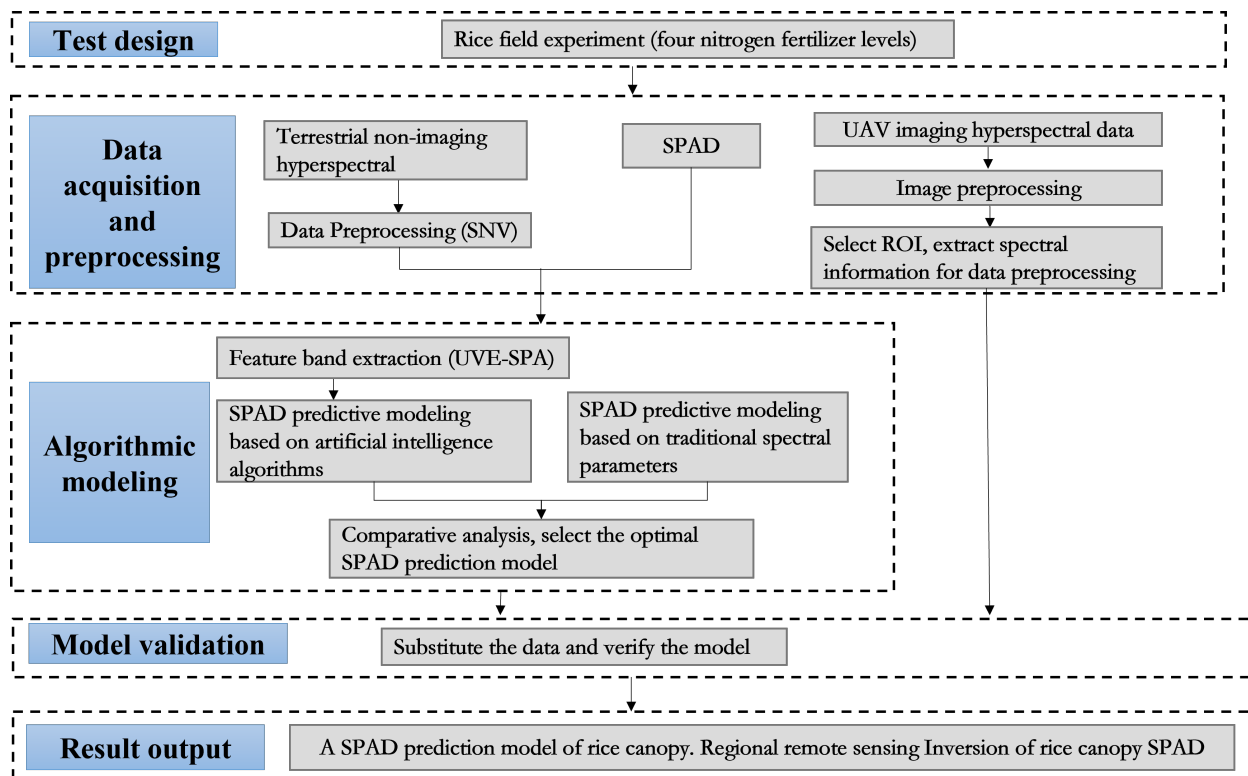


FIGURE 1. Proposed workflow for this study.

MATERIAL AND METHODS

Experimental design

The study area was located in the experimental practice base of Northeast Agricultural University (45°51'N, 127°03'E), Acheng District, Harbin City, Heilongjiang Province, as shown in Fig 2. In this experiment, the crop variety was “Songjing No. 2,” and

four nitrogen application levels were set in the experimental plot, namely N0 (normal nitrogen application), N1 (75% of normal nitrogen application), N2 (50% of normal nitrogen application rate), and N3 (25% of the normal nitrogen application rate). Isolation measures were taken between the experimental plots to prevent the mutual penetration of water and fertilizer between the plots.

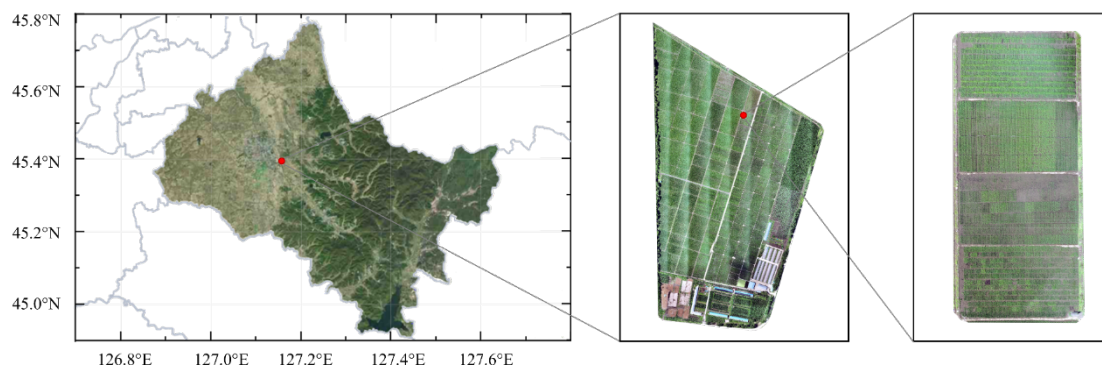


FIGURE 2. Location of the study area.

Experimental data acquisition

The rice seedling transplanting time was May 20, 2021, and the experimental data collection time was July 1 to August 10, 2021. The UAV hyperspectral image data and the corresponding synchronous measurement ground data were collected at the tillering stage, jointing stage, and filling stage of rice. A total of 150 training samples and 50 test samples were obtained.

Nonimaging spectral data

PSR-1100f handheld ground feature spectrometer (hereinafter referred to as PSR-1100f) was used to obtain rice canopy spectrum data. PSR-1100f is a small, convenient, and portable nonimaging spectrometer produced by Spectral Evolution (Mass., USA), which is easy to measure and use in the field. The canopy nonimaging spectroscopy is selected to be carried out in weather with no clouds, clear weather, no wind, or low-wind speed. During the measurement, the instrument was vertically downward, keeping the angle with the normal of the horizontal plane within $\pm 10^\circ$, and the height of the probe from the canopy was about 50 cm. In the experiment, five sets of spectral samples were collected each time, and the latitude and longitude coordinates of the sample points were synchronously collected by differential GPS. Whiteboard calibration is performed before and after spectral data collection to reduce noise and randomness.

UAV hyperspectral image

The DJI Jingwei M300 UAV was synchronously equipped with the S185 imaging spectrometer (hereinafter referred to as S185) for data collection, as shown in Fig 3. S185 is a full-frame, non-scanning, and real-time imaging spectrometer produced by Cubert, Germany. The experiment was carried out under sunny, cloudless, and low-wind conditions. The flying height was 120 m, the heading overlap was set to 80%, and the sideward overlap was set to 70%.



FIGURE 3. DJI M300 UAV and Cubert S185 hyperspectral camera.

SPAD value of rice canopy

A SPAD-502Plus chlorophyll meter was used to simultaneously determine the SPAD of the rice canopy. To reduce the error, 10 SPAD values were uniformly measured on the top three leaves of each sample, and the average value was taken as the SPAD value of the sample, a total of 200 values.

Research methods

Spectral parameters selection

A spectral parameter is a combination of reflectance in specific bands that are related to leaf pigments or photosynthesis, as well as plant water and nutritional status (Yang et al., 2021). This study attempts to construct three types of spectral parameters for remote sensing prediction of SPAD. The names and definitions of the spectral parameters are shown in Table 1.

TABLE 1. Spectral parameter list.

Spectral parameter type	Name	Definition
Vegetation index	Terrestrial chlorophyll index (MTCI)	$(R_{754}-R_{709})/(R_{709}-R_{681})$
	Double-peak Canopy Nitrogen Index (DCNI)	$(R_{722}-R_{702})/(R_{702}-R_{670})/(R_{722}-R_{670}+0.03)$
	Red-edge Normalized Difference Vegetation Index (RNDVI)	$(R_{750}-R_{705})/(R_{750} + R_{706})$
	Red-Edge Position by Linear Interpolation (REPLI)	$700+40(R_{670}-R_{782})/(R_{742}-R_{702})$
	Vogelmann red-edge index (VOG)	R_{742}/R_{722}
Spectral index of any two bands	DSI	R_i-R_j
	RSI	R_i/R_j
	NDSI	$(R_i-R_j)/(R_i+R_j)$

Characteristic bands selection

The original hyperspectral data has the characteristics of multiple bands, large data volume, and strong redundancy. When full-band data is used for modeling, it results in poor modeling efficiency and model performance. Therefore, the hyperspectral data must be reduced in dimensionality (Yuan et al., 2021). This study selects the characteristic bands of the hyperspectral data using the successive projection algorithm (SPA) (MCU et al., 2001) and the uninformed variable elimination (UVE) (Centner et al., 1996) to improve model accuracy and reduce time and model complexity.

Artificial intelligence algorithm

This study compares the three methods of back propagation neural network (BPNN), particle swarm optimization-back propagation neural network (PSO-BPNN), and genetic algorithm-back propagation neural network (GA-BPNN), using the same training set as the spectral parameter method, the SPAD prediction models of rice canopy are constructed respectively, and the accuracy of the models is tested.

Model evaluation method

The coefficient of determination (R^2) and root mean square error (RMSE) are selected as indicators to evaluate the accuracy of training and test. R^2 represents the degree of fitting between the simulated value and the measured value. The closer R^2 is to 1, the higher the accuracy of the fitted curve; the RMSE reflects the degree of deviation between the simulated value and the measured value. The smaller the value, the higher the accuracy of the model.

RESULTS AND DISCUSSION

SPAD prediction analysis and modeling based on spectral parameters

Correlation analysis between the spectral index of any two bands and the rice canopy SPAD

In this experiment, the vegetation index was constructed by using the spectral data in a pairwise combination of arbitrary bands, and the correlation analysis with SPAD was performed respectively, to obtain the R^2 equipotential diagram, as shown in Fig 4, Fig 5.

It can be seen from Fig 4 that the RSI of the combination of 500–526 nm and 450–500 nm and the combination of 450–500 nm and 500–525 nm perform best, and the R^2 reaches 0.60 or more. Among them, RSI (R_{526} ,

R_{469}) has the best correlation with SPAD in rice canopy, and R^2 reaches 0.691.

Figure 5 is an equipotential diagram of NDSI (R_i , R_j) and the SPAD of the rice canopy formed by a combination of any two bands in the range of 450 to 950 nm. For NDSI (R_i , R_j), the region with $R^2 > 0.60$ is a combination of the 680–700 nm and 680–710nm bands. Among them, NDSI (R_{681} , R_{695}) has the best correlation with SPAD, and R^2 reaches 0.685. Compared with RSI (R_i , R_j), NDSI (R_i , R_j) has a narrower band with a better correlation with SPAD and is mostly concentrated in the red-light band. By calculating the R^2 of DSI (R_i , R_j) with the rice canopy SPAD, it is found that DSI (R_i , R_j) is lower than RSI (R_i , R_j) and NDSI (R_i , R_j), and the $R^2 < 0.60$.

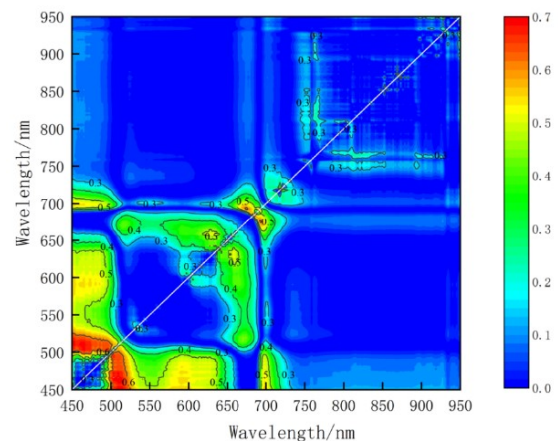


FIGURE 4. Equipotential diagram of R^2 of RSI (R_i , R_j) and SPAD formed by any two bands combination.

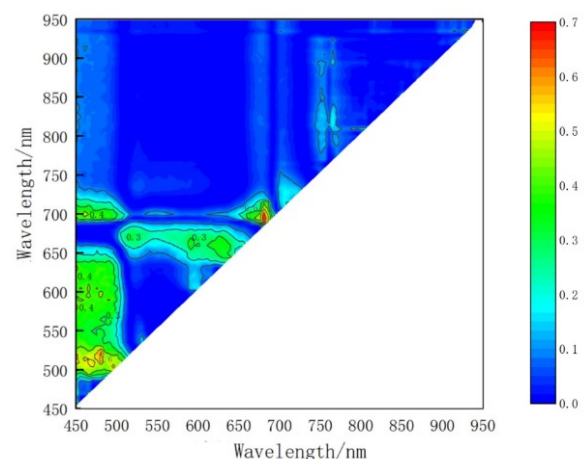


FIGURE 5. Equipotential diagram of R^2 of NDSI (R_i , R_j) and SPAD formed by any two bands combination.

Correlation analysis between typical vegetation index and rice canopy SPAD

In the middle and late stages of rice growth, the time interval between the growth periods is short, and it is easily affected by factors such as the microclimate and moisture of the plot. Therefore, the growth process of rice in different plots will be different. To improve the correlation, this experiment selected five vegetation indices that are less affected by the growth period. Table 2 shows that MTCI with SPAD is significantly correlated and the R^2 is better than the other four vegetation indices. The reason is that the

proposal of MTCI is mainly based on when the concentration of chlorophyll increases, the reflectance difference between R_{709} and R_{681} gradually decreases, while the reflectivity difference between R_{754} and R_{709} is getting bigger and bigger (Dash & Curran, 2007). The vegetation index has the advantages of simple calculation and a strong correlation with chlorophyll content. The other four vegetation indices reflect the chlorophyll content indirectly through other vegetation characteristics, and their performance in correlation analysis with SPAD is not as good as MTCI.

TABLE 2. Correlation of vegetation index with rice canopy SPAD.

Vegetation index	R^2	RMSE
Terrestrial chlorophyll index (MTCI)	0.640	1.765
Double-peak Canopy Nitrogen Index (DCNI)	0.532	2.652
Red-edge Normalized Difference Vegetation Index (RNDVI)	0.506	2.873
Red-Edge Position by Linear Interpolation (REP _{LI})	0.521	2.760
Vogelmann red-edge index (VOG)	0.332	3.762

Construction and analysis of SPAD model in rice canopy based on spectral parameters

In the correlation analysis between the three types of spectral indices and SPAD, the spectral parameters with R^2 greater than 0.60 are selected to construct the unary regression model of each spectral parameter and the rice canopy SPAD. The training set accuracy and test set accuracy of each estimated model are shown in Table 3. The

training set model R^2 of the three models is between 0.609–0.707, and the RMSE is between 0.848–2.894; the test set model R^2 is between 0.640–0.691, and the RMSE is between 0.956–1.965. Among them, the prediction model with RSI (R_{526} , R_{469}) as the input variable has the largest R^2 , the R^2 of the training set reaches 0.70 or more, and the RMSE of the training set and the test set are smaller than other models, and the prediction accuracy is the highest.

TABLE 3. Prediction models of rice canopy SPAD based on spectral parameters.

Spectral parameter	Regression equation	Training set		Test set	
		R^2	RMSE	R^2	RMSE
RSI (R_{526} , R_{469})	$y = 17.34x + 7.329$	0.707	0.848	0.691	0.956
NDSI (R_{681} , R_{695})	$y = 57.036x + 117.263$	0.687	1.008	0.685	1.269
MTCI	$y = 5.475x + 26.65$	0.609	2.894	0.640	1.965

SPAD prediction analysis and modeling based on artificial intelligence algorithm

Selection of characteristic bands

Based on the stability analysis of regression coefficients, the UVE algorithm (Wang et al., 2019) is a new variable selection method. The core of UVE is to add a certain number of random variables into the spectral matrix and establish the PLS model through cross-validation, calculate the ratio (C_i) of the mean value of the regression coefficient to the standard deviation, and remove the invalid spectral information by the size of the ratio. The results of the UVE variable stability analysis are shown in Fig 6. The vertical solid line is the dividing line between the wavelength variable and the random noise variable, the left side is the wavelength variable, and the right side is the random noise variable. The two horizontal dotted lines, respectively, indicate the upper and lower thresholds of the stability of the wavelength variable. The variable stability

threshold is determined by the random noise variable. The variable between the two thresholds can be considered a useless information variable and needs to be eliminated. The other wavelength variables are useful information wavelength variables and will be retained. After the UVE algorithm, a total of 163 wavelength variables are selected.

SPA algorithm is a forward selection algorithm that utilizes a simple projection operation in a vector space to select the subset of variables with the least collinearity and evaluate using RMSE. As an important characteristic wavelength variable extraction algorithm, the SPA algorithm can effectively reduce the collinearity between variables, avoid the repetitiveness of variable information to the greatest extent, and reduce the redundancy between variables. After the UVE algorithm eliminates useless information variables, the SPA algorithm is used to select the remaining wavelength variables. Twelve characteristic bands are selected from the 450–950 nm band, which were 454n, 493, 499, 548, 553, 557, 566, 569, 572, 575, 582, 592 nm.

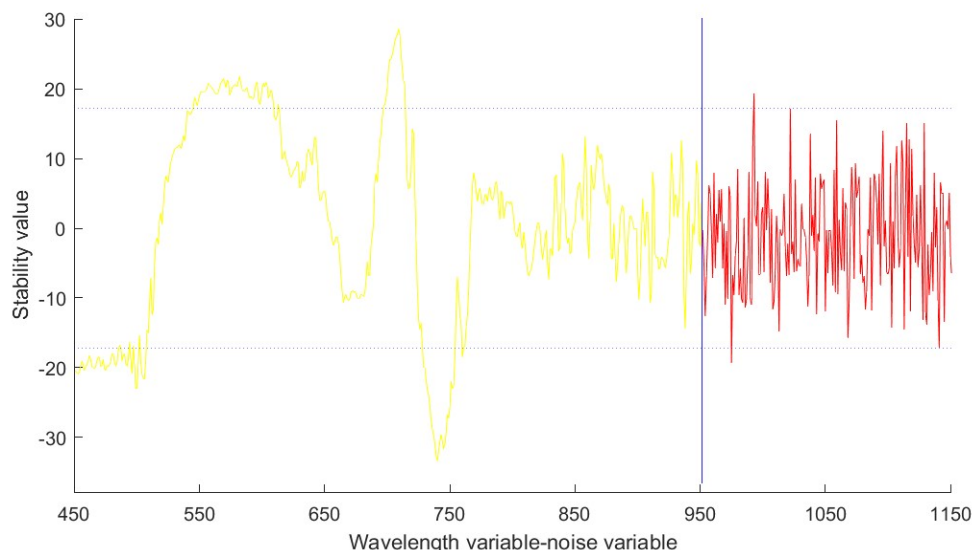


FIGURE 6. Selection of rice canopy characteristic variables based on the UVE algorithm.

BPNN model construction and analysis

BPNN is a multi-layer feedforward neural network trained according to the error back propagation algorithm. The weights and thresholds of the network are continuously adjusted through back propagation to minimize the error square sum of the network (Shao et al., 2021). The twelve characteristic bands selected by the UVE-SPA algorithm are used as the model input, and the rice canopy SPAD is used as the model output to construct the BPNN model. Among them, the transfer function of the hidden layer of the neural network is the tangent sigmoid function (Tansig), the transfer function of the output layer of the neural network is

the linear function Purelin, the training function is Trainlm, the maximum number of training iterations is 10,000, and the learning rate (lr) is 0.0001. In addition, the model predicts the best outcome when there are 15 neurons in the hidden layer after numerous experiments.

The modeling results are shown in Fig 7. The BPNN model has better modeling effects than all prediction models based on vegetation index. The R^2 and RMSE of the model training set are 0.750 and 0.986, respectively. Therefore, the prediction model established by using a combination of 12 characteristic bands as the input of the BPNN has better prediction accuracy.

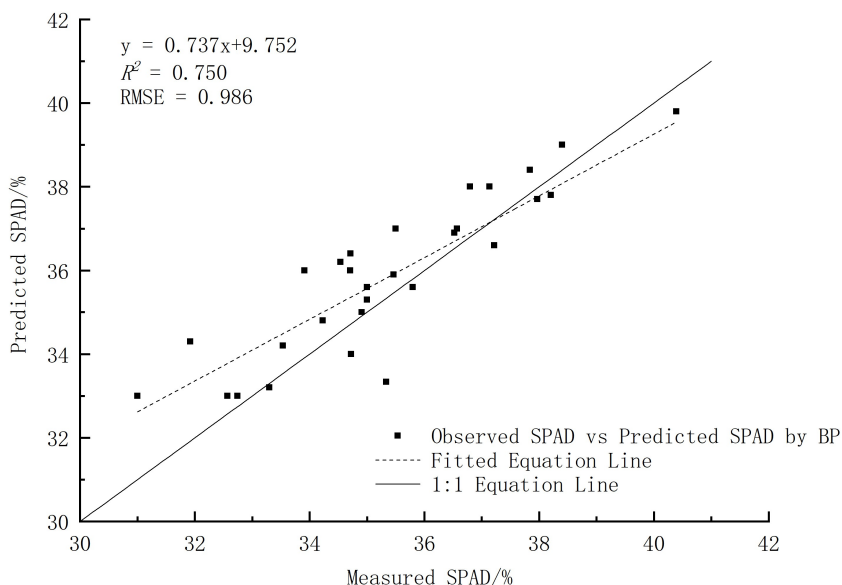


FIGURE 7. Modeling results of BP neural network.

PSO-BPNN model construction and analysis

The idea of PSO (Kennedy & Eberhart, 1995) originated from precursor studies on the way fish and birds flock, which seek the optimal solution through collaboration and information sharing between individuals in the group. The PSO algorithm is used to optimize the weights and

thresholds of the BPNN, thereby reducing the function loss value. The optimization structure is shown in Fig 8.

The 12 characteristic bands selected by the UVE-SPA algorithm are used as the model input, and the rice canopy SPAD is used as the model output to construct the PSO-BPNN prediction model. In the PSO algorithm, the

value of inertia factor β affects the global search ability and convergence ability of particles. This model uses a linearly decreasing inertia weight strategy to determine the inertia factor β , and $\beta = 0.65$. The population size is generally 20–40, and this model takes 30. The learning factors $c1$ and $c2$ determine the influence of the particle's own experience and other particles on the optimal trajectory, which can reflect the information exchange between particles, promoting the exploration and use of search space (Yadav & Anubhav, 2020). A large number of studies point out that the sum of $c1$ and $c2$ is the best at around 4.0, and this model sets $c1=c2=2.15$. The function of the maximum speed limit (V_{max}) is to set the maximum value of the particle speed, thereby limiting the movement distance of the particle. If V_{max} is too large, the particle may jump over the better solution. On the contrary, the particle may not be able to fully explore the space outside the local better solution area, which weakens the global search ability and makes the algorithm fall into the local better solution. In this model,

V_{max} is set to 1. Tansig and Purelin are set as the transfer function of the hidden layer and the output layer, respectively, Trainlm is set as the training function, the maximum number of training iterations is 10,000 times, the learning rate (lr) and the training accuracy are both 0.0001 and 0.01, respectively. At the same time, the model has the best prediction effect when the number of neural nodes in the hidden layer is 15 through step-by-step experiments. The modeling result is shown in Fig 9. The R^2 and RMSE of the PSO-BPNN model are 0.791 and 0.866, respectively. Compared with the BPNN model, the PSO-BPNN model has improved model accuracy and predictive ability, indicating that the use of the PSO algorithm to optimize the BPNN model has higher prediction accuracy for the rice canopy SPAD. The reason is that the particle swarm algorithm has the characteristics of fast search speed, and its information-sharing mechanism enables the population to converge to the maximum value faster.

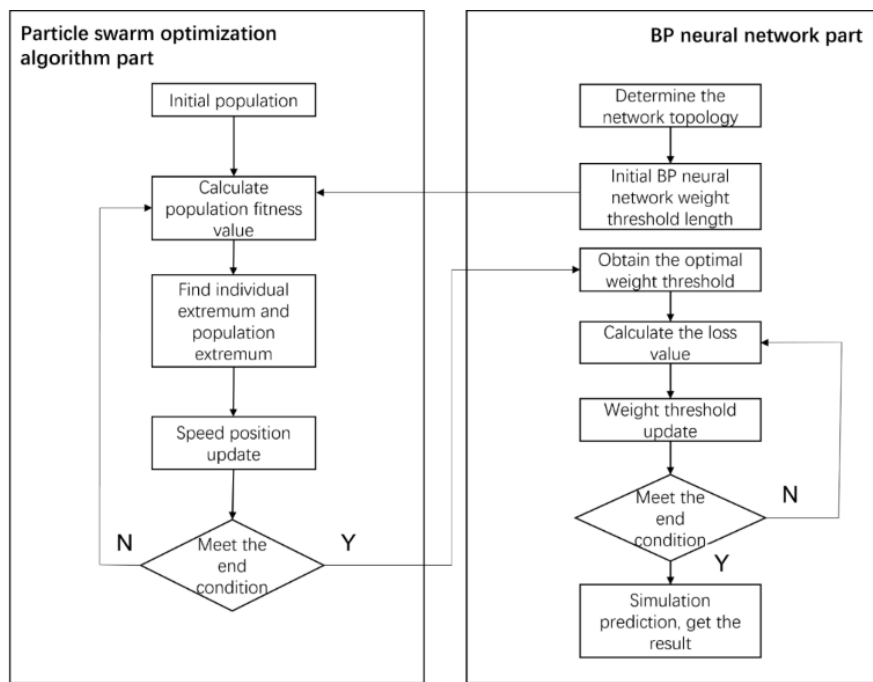


FIGURE 8. PSO-BP neural network flow chart.

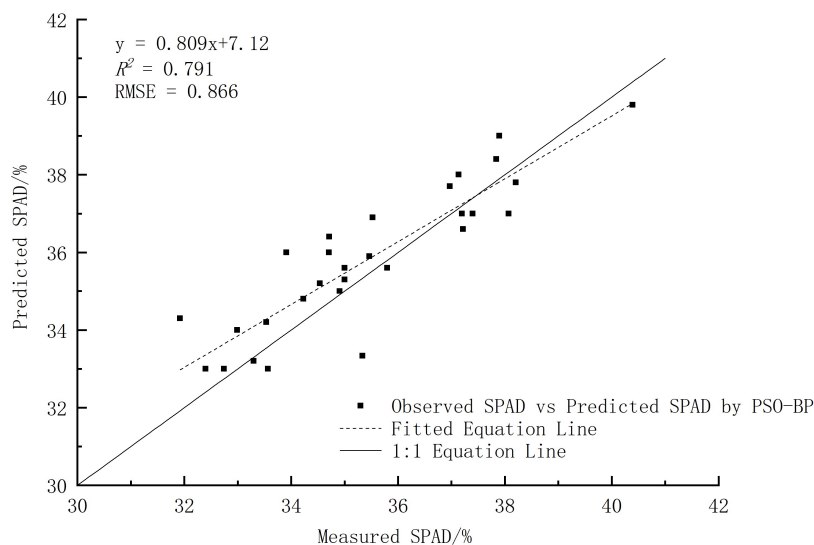


FIGURE 9. Modeling results of PSO-BP neural network.

GA-BPNN model construction and analysis

GA (Abdullah et al., 2020) is an algorithm designed based on the evolutionary laws of the biological world and searches for the optimal solution by simulating the natural evolution process. The main feature of GA is that it can directly operate on structural objects. There is no limitation on function continuity and derivation, and the algorithm uses a probabilistic optimization method, which can automatically obtain and guide the optimized search space. The structure of the BPNN optimized by the GA algorithm is shown in Fig 10.

The 12 characteristic bands selected by the UVE-SPA algorithm are used as the model input, and the rice canopy SPAD is used as the model output to construct the GA-BPNN prediction model. After trial and error, the parameters of the GA-BPNN model are determined: the training function is Trainlm, the transfer function of the output layer is Purelin, the activation function is Sigmoid, the crossover probability is 0.5, the mutation probability is 0.3, and the number of evolutions is 100. At the same time, through step-by-step experiments, it is concluded that when

the number of hidden layer neural nodes is 15, the maximum number of training iterations is 10,000, and the learning rate (Ir) is 0.0001, the prediction effect of the model reaches the best.

The modeling result is shown in Fig 11. The R^2 and RMSE of the GA-BPNN model are 0.818 and 0.847, respectively. Compared with the BPNN model and the PSO-BPNN model, the GA-BPNN model prediction results are closer to the expected value, and the prediction accuracy is higher. The reason is that the GA-BPNN model separately optimizes the weights and thresholds in the process of training, and finds the optimal solution in the global scope, which greatly reduces the prediction error and avoids the neural network from falling to a minimum. At the same time, compared with the weaker stability of the PSO-BPNN, the GA-BPNN is more adaptable. As the number of iterations increases, individual adaptability is also enhanced. Although the accuracy of the GA-BPNN model is improved compared with the PSO-BPNN model, the GA is too computationally expensive in the iterative process, which leads to unsatisfactory real-time prediction results. The model still needs to be optimized and improved.

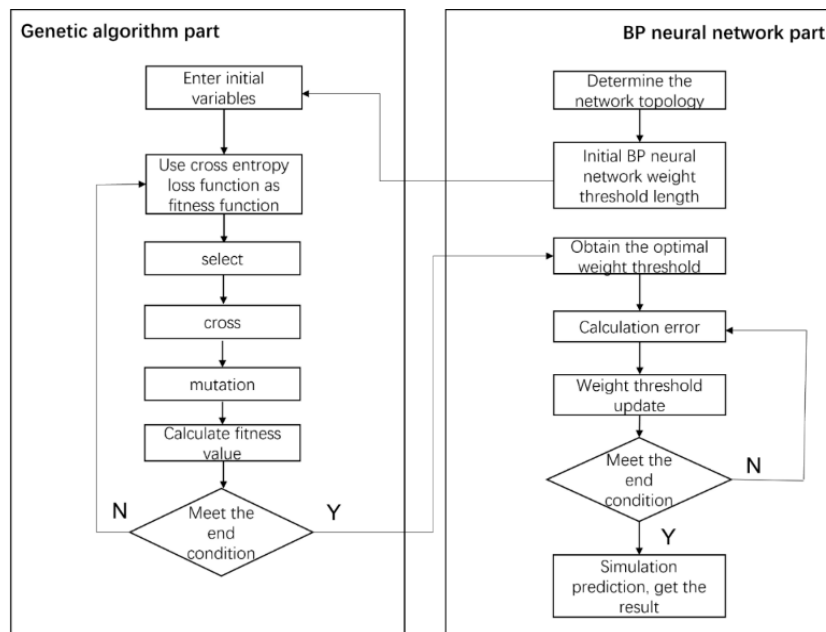


FIGURE 10. GA-BP neural network flow chart.

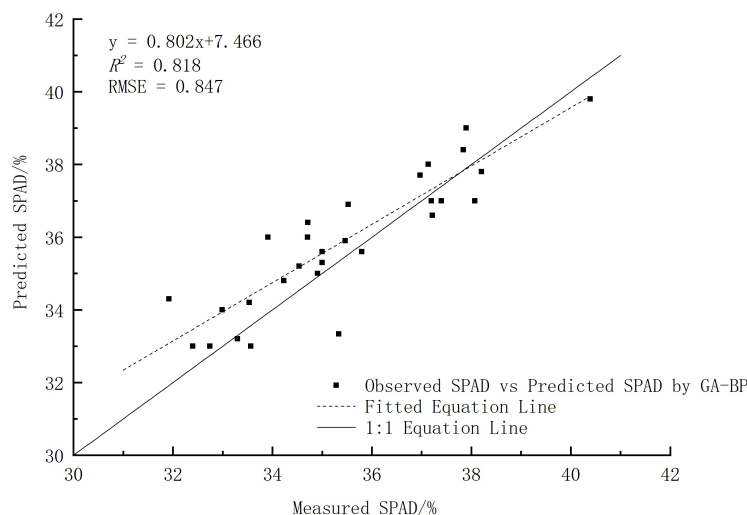


FIGURE 11. Modeling results of GA-BP neural network.

Spatial distribution map of rice canopy SPAD based on imaging spectrum

Comparing the SPAD prediction models of rice canopy constructed by three kinds of neural networks, the GA-BPNN model combined with UAV hyperspectral images is selected to map the cold rice jointing stage SPAD remote sensing inversion mapping. The characteristic bands extracted from each pixel point of the hyperspectral image are used as the input of the GA-BPNN model to obtain the spatial distribution map of rice SPAD in the study area, as shown in Fig 12.

Thirty ground sample points are randomly selected to verify the accuracy. According to the latitude and longitude coordinates of the 30 sample points collected on the ground, the sample points with the same name are found on the map. The ground SPAD measured values of these

sample points are fitted and analyzed with the predicted values of the points with the same name on the spatial distribution map. The results are shown in Fig 13. The R^2 of the fitting equation is 0.789, and the RMSE is 0.986. Compared with the use of ground spectral information to build the GA-BPNN model (Fig 9), the accuracy is lower. The main reason is that the establishment of the model is based on ground nonimaging spectral data, while the UAV verification data uses imaging spectral data. The two sensors are different, resulting in differences in spectral information. In addition, during the verification, there is a certain error in the corresponding relationship between the measured value on the ground and the point of the same name in the image, which causes the accuracy of the model verification to be reduced. In summary, combining ground spectral information and UAV images can achieve high-precision regional rice SPAD inversion.

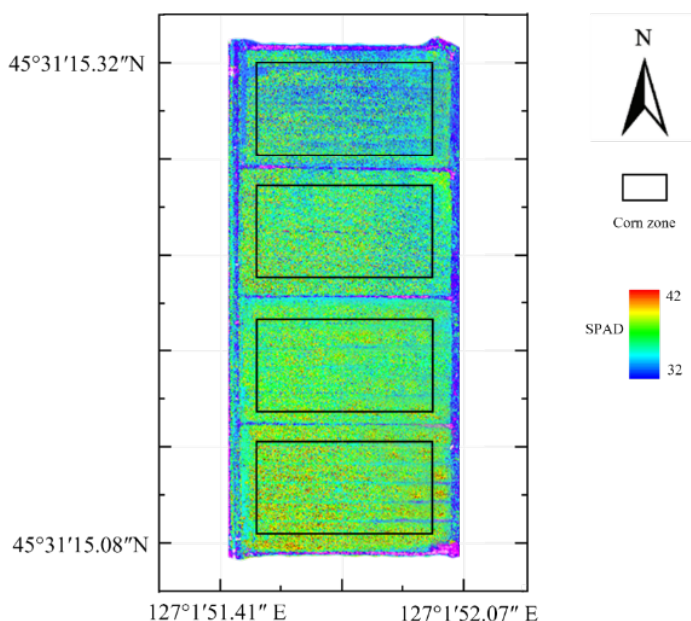


FIGURE 12. Retrieved rice canopy SPAD at jointing stage in the study area.

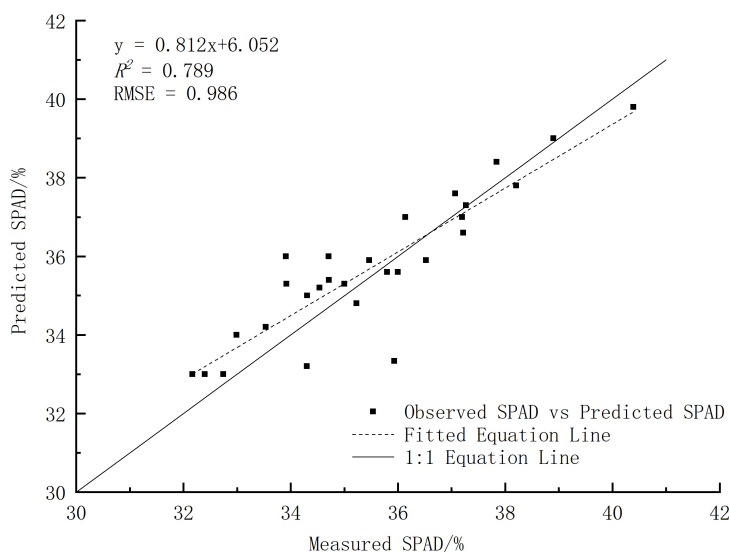


FIGURE 13. Relationship between measured and predicted SPAD value of test samples on predicted SPAD map.

In recent years, excessive chemical fertilizer application or nitrogen deficiency in rice production in Heilongjiang Province have resulted in a decline in rice quality and low nitrogen utilization efficiency. Peng et al (2019) studied the fertilization situation of rice fields in Heilongjiang Province, and the results showed that only 20% of the farmland can achieve high yield and high efficiency. Although many previous studies on the effects of nitrogen utilization and SPAD on crop yield, photosynthetic characteristics, and root growth have been conducted, the majority of these studies have been conducted in southern regions. There are relatively few studies in the northeast cold region. Therefore, we studied four types of rice with different ammonia fertilizers under the local traditional cultivation mode and developed a SPAD prediction model to provide a theoretical foundation for rational nitrogen application and rice yield improvement in cold regions.

In monitoring rice biophysical and chemical parameters, the spectral parameter method has some advantages. Therefore, many researchers have proposed a variety of wavelength-based selection methods for predicting rice SPAD, nitrogen content, and LAI (Liu et al., 2010; Ryu et al., 2009; Gao et al., 2016).

This study uses arbitrary band combinations to construct the vegetation index RSI and NDSI, calculates the correlation between the vegetation index and SPAD, selects the optimal band combination, and calculates the correlation between five typical vegetation indices and SPAD. The SPAD prediction models of rice canopy in the cold region are constructed with better spectral parameters. Among them, RSI (R_{526} , R_{469}), NDSI (R_{681} , R_{695}), and MTCI perform well, and the R^2 is all greater than 0.60.

The three neural network models have simpler structures, stronger correlations with SPAD, and higher accuracy when compared to spectral parameter models. The R^2 of the five spectral parameter models are all lower than the three neural network models, and the optimal RSI (R_{526} , R_{469}) model has an R^2 of 0.707, which is 0.111 lower than that of the GA-BPNN model. The reason for this is that predicting biophysical and chemical parameters using spectral parameters will be influenced by factors such as soil background and atmosphere, giving the model territoriality and temporality. In this study, the BPNN can improve the accuracy of estimation, and the prediction effect is better than the traditional vegetation index model, which is consistent with the results of previous studies (Xia et al., 2013). The three neural network models do not require a specific mathematical model in data processing, and the simulation is strong, resulting in better interpretability for nonlinear problems.

When comparing the three neural network models, the GA-BPNN model outperforms the BPNN and PSO-BPNN models in terms of prediction. The reason for this is that the GA can optimize the weights and thresholds separately, find the optimal solution in the global scope, and improve the prediction accuracy and robustness of the BPNN model. The R^2 of the GA-BPNN model is 0.818, which is 0.027 higher than that of the PSO-BPNN. However, because the GA has issues such as slow speed and a long iterative process, the model still has a lot of room for improvement. The focus of the next step is to combine

artificial intelligence algorithms with traditional spectral parameter methods to monitor crop biophysical and chemical parameters and to obtain models with the higher predictive ability and better robustness.

CONCLUSIONS

In this study, the canopy hyperspectral and SPAD data of rice in a cold region are obtained through field experiments, which are modeled based on spectral parameters and artificial intelligence algorithms, respectively. The conclusions obtained are as follows.

(1) The correlation between the spectral index RSI (R_{526} , R_{469}) selected by any two bands and the SPAD of the cold rice canopy is better than that of the five typical vegetation indices, with R^2 reaching 0.691 and RMSE being 0.956. However, the prediction accuracy of this model is worse than that of the GA-BPNN model, and it can only roughly estimate the SPAD of the rice canopy.

(2) The GA-BPNN model is the optimal prediction model for SPAD of rice canopy in a cold region. The R^2 of the prediction model reaches 0.818, which can predict SPAD well. The prediction range (33.1–41.2) of rice canopy SPAD at the jointing stage based on UAV hyperspectral images is in good agreement with the measured value on the ground (32.7–40.6), which can realize the SPAD remote sensing mapping within the region, and provide scientific guidance and technical support for the management of rice production in a cold region.

ACKNOWLEDGMENTS

This study was supported by the auspices of the central government supports the reform and development of local colleges and universities in Heilongjiang Province (2020GSP15), and Heilongjiang Province "hundred thousand million" project science and technology major project (2019ZX14A04).

REFERENCES

- Abdullah S, Pradhan, RC, D Pradhan, Mishra S (2020) Modeling and optimization of pectinase-assisted low-temperature extraction of cashew apple juice using artificial neural network coupled with genetic algorithm. *Food Chemistry* 339(2-3):127862. DOI: <https://doi.org/10.1016/j.foodchem.2020.127862>
- Centner V, Massart DL, Denoort OE, Dejong S, Vandeginste BM, Sterna C (1996) Elimination of uninformative variables for multivariate calibration. *Analytical Chemistry* 68(21):3851-3858. DOI: <https://doi.org/10.1021/ac960321m>
- Dash J, Curran PJ (2017) Evaluation of the meris terrestrial chlorophyll index (MTCI). *Advances in Space Research* 39(1):100-104. DOI: <https://doi.org/10.1016/j.asr.2006.02.034>
- Gao L, Yang G, Yu H, Xu B, Zhao X, Dong J, Ma Y (2016) Retrieving winter wheat leaf area index based on unmanned aerial vehicle hyperspectral remote sensing. *Transactions of the Chinese Society of Agricultural Engineering* 32(22):113-120. DOI: <https://doi.org/10.11975/j.issn.1002-6819.2016.22.016>

- Guo B, Qi S, Heng Y, Duan J, Zhang H, Wu Y, Feng W, Xie Y, Zhu Y (2016) Remotely assessing leaf nitrogen uptake in winter wheat based on canopy hyperspectral red-edge absorption. *European Journal of Agronomy* 82(part_PA): 113-124. DOI: <https://doi.org/10.1016/j.eja.2016.10.009>
- He Y, Zhao X, Zhang W, He X, Tong L (2021) Study on the identification of resistance of rice blast based on near infrared spectroscopy. *Spectrochimica Acta Part A: Molecular and Biomolecular Spectroscopy* 266(2022): 120439. DOI: <https://doi.org/10.1016/j.saa.2021.120439>
- Inoue Y, Sakaiya E, Zhu Y, Takahashi W (2012) Diagnostic mapping of canopy nitrogen content in rice based on hyperspectral measurement. *Remote Sensing of Environment* 126: 210-221. DOI: <https://doi.org/10.1016/j.rse.2012.08.026>
- Jiang H, Yang H, Chen X, Wang S, Li X, Liu K, Cen Y (2015) Research on accuracy and stability of inverting vegetation chlorophyll content by spectral index method. *Spectroscopy & Spectral Analysis*. 35(4):975-981. DOI: [https://doi.org/10.3964/j.issn.1000-0593\(2015\)04-0975-07](https://doi.org/10.3964/j.issn.1000-0593(2015)04-0975-07)
- Kennedy J, Eberhart R (1995) Particle swarm optimization. In: *ICNN'95 International Conference on Neural Networks*. Perth, IEEE, Proceedings...
- Li X, Liu X, Liu M, Wu L (2014) Random forest algorithm and regional applications of spectral inversion model for estimating canopy nitrogen concentration in rice. *Journal of Remote Sensing* 18(4):934-945. DOI: <https://doi.org/10.11834/jrs.20142329>
- Liu H, Zhu H, Li Z, Yang G (2014) Quantitative analysis and hyperspectral remote sensing of the nitrogen nutrition index in winter wheat. *International Journal of Remote Sensing* 41(1):1-24. DOI: <https://doi.org/10.1080/01431161.2019.1650984>
- Liu M, Liu X, Li M, Fang M, Chi W (2010) Neural-network model for estimating leaf chlorophyll concentration in rice under stress from heavy metals using four spectral indices. *Biosystems Engineering* 106(3):223-233. DOI: <https://doi.org/10.1016/j.biosystemseng.2009.12.008>
- Ma D, Maki H, Neeno S, Zhang L, Jin J (2010) Application of non-linear partial least squares analysis on prediction of biomass of maize plants using hyperspectral images. *Biosystems Engineering* 200:40-54. DOI: <https://doi.org/10.1016/j.biosystemseng.2020.09.002>
- Araújo MCU, Saldanha TCB., Galvão RKH, Yoneyama T, Chame HC, Visani V (2001) The successive projections algorithm for variable selection in spectroscopic multicomponent analysis. *Chemometrics & Intelligent Laboratory Systems* 57:65-73. DOI: [https://doi.org/10.1016/S0169-7439\(01\)00119-8](https://doi.org/10.1016/S0169-7439(01)00119-8)
- Peng X, Wang W, Zhou N, Liu H, Li P, Liu Z, Yu C (2019) Analysis of fertilizer application and its reduction potential in paddy fields of Heilongjiang Province. *Scientia Agricultura Sinica* 52(12). DOI: <https://doi.org/10.3864/j.issn.0578-1752.2019.12.007>
- Ryu C, Suguri M, Umeda M (2009) Model for predicting the nitrogen content of rice at panicle initiation stage using data from airborne hyperspectral remote sensing. *Biosystems Engineering* 104(4):465-475. DOI: <https://doi.org/10.1016/j.biosystemseng.2009.09.002>
- Shao W, Guan Q, Tan Z, Luo H, Ma Y (2021) Application of BP-ANN model in evaluation of soil quality in the arid area, northwest China. *Soil and Tillage Research* 208(2): 104907. DOI: <https://doi.org/10.1016/j.still.2020.104907>
- Song D, Gao D, Sun H, Qiao L, Zhao R, Tang W, Li M (2021) Chlorophyll content estimation based on cascade spectral optimizations of interval and wavelength characteristics. *Computers and Electronics in Agriculture* 189(1):106413. DOI: <https://doi.org/10.1016/j.compag.2021.106413>
- Tan K, Wang S, Song Y, Liu Y, Gong Z (2017) Estimating nitrogen status of rice canopy using hyperspectral reflectance combined with BPSO-SVR in cold region. *Chemometrics and Intelligent Laboratory Systems* 172:68-79. DOI: <https://doi.org/10.1016/j.chemolab.2017.11.014>
- Tang Y, Wang R, Huang J, Kong W, Cheng Q (2004) Hyperspectral data and their relationships correlative to the pigment contents for rice under different nitrogen support level. *Journal of Remote Sensing* 8(2):185-192. DOI: <https://doi.org/10.3321/j.issn:1007-4619.2004.02.014>
- Wang Z, Chen J, Fan Y, Cheng Y, Wu X, Zhang J, Wang B, Wang X, Yong T, Liu W, Liu J, Du J, Yang W, Yang F (2019) Evaluating photosynthetic pigment contents of maize using UVE-PLS based on continuous wavelet transform. *Computers and Electronics in Agriculture* 169:105160. DOI: <https://doi.org/10.1016/j.compag.2019.105160>
- Wen P, He J, Ning F, Wang R, Zhang Y, Li J (2019) Estimating leaf nitrogen concentration considering unsynchronized maize growth stages with canopy hyperspectral technique. *Ecological Indicators* 107: 105590. DOI: <https://doi.org/10.1016/j.ecolind.2019.105590>
- Xia T, Wu W B, Zhou QB, Zhou Y (2013) Comparison of two inversion methods for winter wheat leaf area index based on hyperspectral remote sensing. *Transactions of the Chinese Society of Agricultural Engineering* 2013(3): 139-147. DOI: <https://doi.org/10.3969/j.issn.1002-6819.2013.03.019>
- Xu T, Guo Z, Yu F, Xu B, Feng S (2020) Genetic algorithm combined with extreme learning machine to diagnose nitrogen deficiency in rice in cold region. *Transactions of the Chinese Society of Agricultural Engineering* 36(2): 209-218. DOI: <https://doi.org/10.11975/j.issn.1002-6819.2020.02.025>
- Yadav R, Anubhav (2020) PSO-GA based hybrid with Adam optimization for ANN training with application in medical diagnosis. *Cognitive Systems Research* 64:191-199. DOI: <https://doi.org/10.1016/j.cogsys.2020.08.011>

Yang F, Liu T, Wang Q, Du M, Yang T, Liu D, Li S, Liu, S (2020) Rapid determination of leaf water content for monitoring waterlogging in winter wheat based on hyperspectral parameters. *Journal of Integrative Agriculture* 20(10):2613-2626. DOI: [https://doi.org/10.1016/S2095-3119\(20\)63306-8](https://doi.org/10.1016/S2095-3119(20)63306-8)

Yuan R, Liu G, He J, Wan G, Fan N, Li Y, Sun Y (2020) Classification of Lingwu long jujube internal bruise over time based on visible near-infrared hyperspectral imaging combined with partial least squares-discriminant analysis. *Computers and Electronics in Agriculture* 182(7–8):106043. DOI: <https://doi.org/10.1016/j.compag.2021.106043>

Yue J, Yang G, Tian Q, Feng H, Xu K, Zhou C (2019) Estimate of winter-wheat above-ground biomass based on UAV ultrahigh-ground-resolution image textures and vegetation indices. *ISPRS Journal of Photogrammetry and Remote Sensing*. 150:226-244. DOI: <https://doi.org/10.1016/j.isprsjprs.2019.02.022>

Zhu W, Sun Z, Gong H, Li J, Zhu K (2020) Estimating leaf chlorophyll content of crops via optimal unmanned aerial vehicle hyperspectral data at multi-scales. *Computers and Electronics in Agriculture* 178:105786. DOI: <https://doi.org/10.1016/j.compag.2020.105786>